

MC-TH-98-17

October 1998

Revised: December 1998

New explanation of the strange baryon rapidity distributions in ultra-relativistic nucleus-nucleus collisions.

J. A. Casado ¹

Department of Physics and Astronomy,
University of Manchester,
Manchester, M13 9PL, England.

Abstract

A model of multiparticle production in hadronic collisions at ultra-relativistic energies, based on the assumption of independent string fragmentation, reproduces the rapidity spectra of Λ and $\bar{\Lambda}$ in sulphur-sulphur collisions reported by the NA35 Collaboration. This is achieved after a reconsideration of the intermediate multi-string states and the structure of the diquarks. Nuclear stopping power is also studied through the computation of the $p - \bar{p}$ rapidity spectra.

¹ E-mail: casado@a13.ph.man.ac.uk

1 Introduction

Strange particle production in heavy ion collisions is a subject of great interest since it may provide evidences of the formation of a new state of matter: the quark-gluon plasma (QGP). The tantalizing pursuit of this discovery is the justification for the efforts being made to carry out the heavy-ions collision experiments that have taken place at the AGS and CERN-SPS, and to plan new ones for future facilities. A phase transition between normal nuclear matter to a deconfined phase has been predicted long ago^[1, 2] to occur at very high temperatures and densities. For the time being, the properties of the QGP have not being clearly stabilised, neither the order of the phase transition between the two states. This makes the problem of recognizing the formation of QGP, if it happens, particularly difficult, more so since we have to rely on indirect clues to its detection. Several signatures have been proposed for this purpose that may deliver circumstantial evidences of the formation of quark matter (for an up-to-date review on the subject with a complete list of references, see [3]). The strange mesons, baryons and antibaryons production has been predicted to be greatly enhanced in the presence of QGP as compared to the case when there are only standard hadron matter^[4, 5]. Also the study of the stopping power may help to uncover the presence of the deconfined phase: a rapid change in the shape of the rapidity baryon distributions with increasing incident beam energy is thought to be a clear signal for new degrees of freedom^[6].

An additional problem is caused by the lack of a full description of the confined phase, which constitutes the background to the events in which QGP may have been formed. *Enhanced strange particle production* is a meaningless expression unless we can find out what strange particle production must be expected from an ordinary ion-ion collision event. We can not extract this information from QCD since we do not know how to apply this theory when the effective coupling constant is not small. This is also the ultimate cause of the lacunae in our understanding of the QGP properties and of the order of the phase transition mentioned in the above paragraph. We have to rely on phenomenological models to fill this gap. The Dual Parton Model (DPM)^[7] and the Quark Gluon String Model (QGSM)^[8, 9] have been very successful in describing many features of hadron-hadron, hadron-nucleus and nucleus-nucleus collisions. Nevertheless, they were not able to reproduce^[10] the rapidity distributions of Λ and $\bar{\Lambda}$ hyperons, as well as proton minus antiprotons ($p - \bar{p}$), in central sulphur-sulphur collisions measured by the NA35 Collaboration^[11, 12]. The idea that the onset of the deconfinement phase transition may be at the origin of this disagreement is very appealing. However, we must carefully explore any other possible explanation of these data before admitting that eventuality. The NA35 data show a large production of Λ 's in the fragmentation as well as in the central region. It is very difficult to understand why the formation of QGP in a collision between identical nuclei should contribute so largely to the borders of the accessible phase space. Furthermore, the energy densities currently available at the AGS and CERN-SPS of $0.5\text{-}10 \text{ GeV/fm}^2$ correspond to temperatures between 100 and 200 MeV^[13], for which the effective coupling constant of QCD is not less than 1. Under these condition we can not but look at the possibility of deconfinement with scepticism.

Strangeness enhancement is also present in pp interactions. The ratio K/π increases both with the energy of the collision and with the multiplicity^[14]. It has also been observed an increase of the ratio $\bar{\Lambda}/\bar{p}$ in pp collisions as the centre-of-mass energy increases from 20 GeV to 1800 GeV^[15]. Again, the NA35 Collaboration also reported that strangeness is enhanced between pp

and pS collisions^[11]. This suggests that the nucleon-nucleon rescattering may be at the heart of this phenomena. Indeed, the average number of collisions per participant nucleon increases between pp and pA collisions as well as between pA and central AB collisions. According to the DPM and the QGSM, the extra particles are produced by the fragmentation of strings that have sea quarks at their ends. As this mechanism on its own failed to reproduce the observed enhancement of Λ and $\bar{\Lambda}$ in central SS collisions, additional sources of this increase have been explored.

Diquark-antidiquark pairs from the nucleon sea have been introduced^[16, 17, 18]. This mechanism predicts, contrary to the experimental evidence, the same increase in absolute value of strange baryons and antibaryons. In reference [10] the problem is treated considering final state interactions of co-moving pions and nucleons of the type $\pi + N \rightarrow K + \Lambda$. This approach is not convincing since it contains the unrealistic assumption that all baryons are created instantaneously at the beginning of the collision.

What the data on strange baryon production of the NA35 Collaboration may actually be suggesting is that we are missing an important piece in our understanding of the nucleon-nucleon rescattering. I devote this paper to reconsider how the valence and sea quarks take part in the formation of the ends of strings. I will show that, by allowing the diquarks be formed not only of valence quarks, a good understanding of the data is obtained. In order to do this, in section 2 I discuss the theoretical basis of the paper and make a full description of the model. The next two sections deal with fits to pp data to obtain the value of some parameters of the model, and the results for nucleus-nucleus collision. The paper ends discussing the conclusions.

There are a number of other models that are also constructed around the idea of independent fragmentation of strings. The best known is the Lund-Fritiof model^[19]. Although the general assumptions are at first sight very similar to the ones in DPM and QGSM, the theoretical basis from which these models were developed are quite different and I will not refer to them in the rest of the paper.

2 The Model

The independent-fragmentation string models, DPM and QGSM, were inspired by the developments of the Dual Topological Unitarization (DTU)^[20, 21, 22, 23, 24]. The amplitudes of high-energy hadronic collisions were formally written as an expansion in powers of $1/N_f$, where N_f is the number of flavours. Each term in the expansion can be associated with a diagram with definite topology. The scheme was based on the S-matrix analysis and was closely related to the Regge Field Theory (RFT). The DTU program was reinforced when Veneziano^[25] established a conceptual link with QCD as he included in the series powers of $1/N_c^{[26, 27, 28]}$, being N_c the number of colours. In this way, the whole series of the topological expansion formally includes all the terms of the perturbative QCD series ensuring unitarity.

The lowest order term corresponds to a planar diagram connecting two colliding-hadron lines. Although we will normally choose to make the representations in momentum (rapidity) space, it is illustrative to draw the process in coordinate space. For instance, a $\pi\pi$ collision can be described as a process in which one constituent quark from one pion annihilates with an antiquark from the other pion. The two remaining hadron fragments interact through the colour field that, due to confinement, tends to occupy the smallest possible volume in a quasi

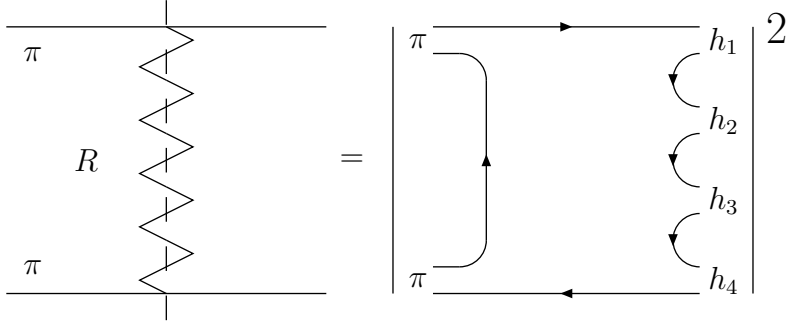


Figure 1: Representation of a cut reggeon and its relation with the planar diagram.

one-dimensional configuration. This colour string stretches between both hadronic fragments and, if we consider the process in Minkowski space, sweeps a two dimensional surface. By the nature of this structure, in the center-of-mass reference frame, the fastest parts of the string are at the edges and the slowest at the centre. This provides a correlation between rapidity and position along the string axis. In the case of an elastic interaction this string decays into a quark-antiquark pair that appears in the final state as part of two pions identical to the initial ones. The representation of a planar inelastic process is obtained applying the optical theorem by considering cuts through the corresponding elastic diagram as depicted in fig. 1. The planar diagram corresponds to the exchange in the t channel of an object that, in terms of internal quantum numbers, is equivalent to a $q - \bar{q}$ system (or a $qq - \bar{q}\bar{q}$ system as happens with one of the two components of the $p - \bar{p}$ planar elastic scattering). This corresponds to the exchange of a reggeon. As a consequence of the topology of the system we can assume that the final particle state in an inelastic collision would possess some characteristic features, such as a one dimensional arrangement of the produced hadrons, short-range rapidity correlation and strong order in longitudinal momentum space. Under the low- p_T exchange assumption, this configuration would approximately have the direction of the collision axis.

At this point, unitarity requires the inclusion of all diagrams obtained by repeatedly multiplying the planar term by itself. The next order topology we have to consider is that of the cylinder. From the physical point of view, this corresponds to the situation in which no constituent quarks or diquarks are annihilated. The colour field forms two strings of the same nature as the one in the planar case. In an inelastic collision both strings decay independently. If the collision is elastic, they annihilate each other as the colour fields in the strings have opposite orientations. It is also clear that only vacuum quantum numbers can be transferred between the interacting hadrons. It is straightforward to realize that this interaction corresponds to the exchange of a pomeron, being the corresponding inelastic cross section obtained cutting through the one pomeron exchange diagram (see fig. 2). Higher order terms can be obtained by combining the simplest topologies described above, and all of them have a one to one correspondence with Reggeon Field Theory (RFT) diagrams. Bearing in mind that we are interested in the high-energy regime, we make use of this correspondence to neglect terms containing the exchange of one or more reggeons: although they may be dominant in the

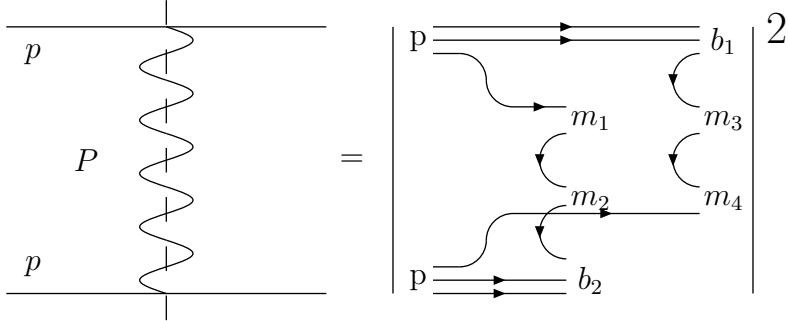


Figure 2: Diagrammatic representation of a cut pomeron and its relation with the cylinder diagram.

topological expansion, their contribution decreases with the centre-of-mass energy squared s as $s^{\alpha_R(0)-1} \sim s^{-0.5}$ while the pomeron exchange subdiagrams behaves like $s^{\alpha_P(0)-1} = s^\Delta$, where $\Delta \geq 0$.

This formal developments laid the foundation of phenomenological models that had to fill the conceptual gaps left by the theory. Both DPM and QGSM postulated that multiparticle production in hadronic collisions at ISR energies, take place in two definite steps. First, the hadrons split in two fragments that share the total momentum of the hadron according to the corresponding structure functions. One of the fragments belongs to the 3 representation of the $SU(3)$ colour group, a quark, and the other to the $\bar{3}$ representation, an antiquark in the case of a meson or a diquark in the case of a baryon. Secondly, two colour strings are formed each one having a fragment of the 3 representation in one end from one of the hadrons, and another of the $\bar{3}$ representation, from the other hadron at the other end. These two strings decay into two chains of hadrons that form the final multiparticle state. The contribution of a string to the final state is given by the fragmentation functions that are, along with the structure functions, the other basic ingredient of the models.

When we move to higher energies, we have to introduce terms with more than two strings that correspond to diagrams with several cut pomerons. The probability weights of the different diagrams are given by the perturbative RFT that can be effectively described by a generalized eikonal model^[7]. Each cut pomeron add two chains of hadrons to the final state as the result of the decay of two more strings. The generalization of the models to hadron-nucleus and nucleus-nucleus collisions carries some similarities with this extrapolation to higher energies. In this case, multiple inelastic collision appears as a consequence of the rescattering of each nucleon by the nucleons on the other interacting nucleus. Again, for each additional inelastic collision we have to consider the fragmentation of two extra chains. The probability weights are given in this case by an external model like that of Glauber-Gribov, that reproduces the geometry of the collision.

Both DPM and QGSM assume that the diquarks at the end of the strings in hadronic collisions, are always made of valence quarks. So, in the case of a colliding proton, regardless of the number of cut pomerons in the collision, the diquark can only be of type (uu) or (ud). The

central point to this paper is the assumption that the sea quarks can be part of the diquark with the same probability as the valence quarks. It is still true that the diquark in a proton can only be of the types mentioned above when it suffers only one inelastic collision. But, when the number of cut pomerons is greater than one, we also have to consider diquarks of the type (dd) , (us) , (ds) and (ss) . The flavour content of the diquark depends on the flavour content of the hadron sea.

This assumption means the inclusion of terms of the topological expansion that are missing in the other independent strings fragmentation models. They correspond to diagrams where the cylinder (the pomeron) is linked to the colliding hadron through a $q^v\bar{q}^s$ or \bar{q}^vq^s trajectory as depicted in fig. 3(b). For the incoming nucleon to interact with two nucleons of the target it is necessary that it appears in a virtual state composed of a baryon-like and a meson-like states. Then, the topology of the interaction can be depicted as the superposition of a baryon-nucleon and a meson-nucleon collisions. In other models, the baryon-like state could only be formed with the three valence quarks, and only meson-like states of the type $|u\bar{u}\rangle$, $|d\bar{d}\rangle$, etc, where considered. I am dropping this restriction only justified for high-mass intermediate states, where sea quark-antiquark pairs are created with large values of rapidity (> 1) respect to their parent hadron. Therefore, in a proton - nucleus collision we now have to include, besides $|p^*\pi^{0*}(\rho, \dots)\rangle$, states like $|\Lambda^* K^{+*}\rangle^2$.

These new components enhance the production of the strange baryons in the fragmentation region due to the contribution of strange diquark fragmentation. I consider a theory with only three flavours: u , d and s , and assume that the u and d contents of the sea are equal, while the s content is suppressed and represented by the parameter S .

$$S = \frac{2\bar{s}}{\bar{u} + \bar{d}} \quad . \quad (1)$$

SU(3) symmetry corresponds to a value $S = 1$. I take $S = 0.5$ that is compatible with several data analysis^[15, 29, 30]. In the rest of the paper, I will be using γ as the portion of strange sea-quarks over the total number of sea-quarks:

$$\gamma = \frac{\bar{s}}{\bar{u} + \bar{d} + \bar{s}} = \frac{S}{S + 2} \quad . \quad (2)$$

For the given value of S , $\gamma = 0.2$.

2.1 Structure Functions

The only essential difference between the DPM and the QGSM comes from the way they postulate the structure functions for sea quarks and antiquarks. Only the leading behaviour at $x \rightarrow 0$ is retained in all cases, that has been called the *retardation* of the hadron fragments. In a collision in which there is only one cut pomeron, the retardation of a quark of flavour f depends on the intercept of the corresponding $q^f\bar{q}^f$ trajectory while for the diquark depends on the intercept of the corresponding $qq\bar{q}\bar{q}$ exotic trajectory. When dealing with nucleons, for these functions we have

$$f_{q^v}(x) = x^{-\alpha_R}, \quad f_{qq}(x) = x^{\alpha_R(0)-2\alpha_N(0)} \quad . \quad (3)$$

² *Baryon-like* and *meson-like*, as well as the asterisks, mean that they are not real baryons or meson since only the flavour content is considered and no attention is paid to other quantum numbers

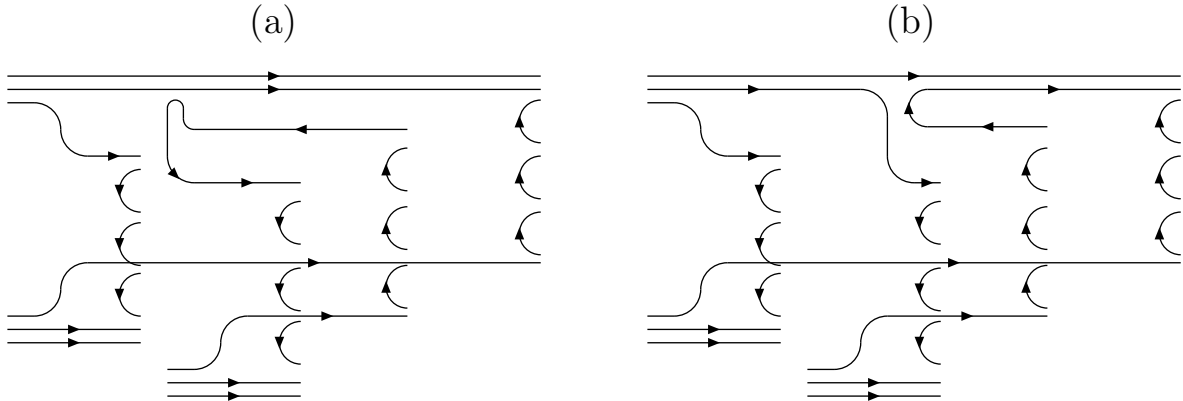


Figure 3: Two diagrams corresponding to inelastic collisions of a nucleon with two nucleons from the target. Diagram (a) is common to all models, while diagram (b) is one of the new components considered in this paper.

Where we have made use of the equation, valid in the planar approximation, $\alpha_{q^a q^b \bar{q}^a \bar{q}^b} + \alpha_{q^c \bar{q}^c} = 2\alpha_{q^a q^b q^c}$ and $\alpha_R(0)$ ($\alpha_N(0)$) is the zero intercept of the leading Regge (nucleon) trajectory.

When there are more than one cut pomeron, we need quarks and antiquarks from the sea to make up enough string ends. In the DPM, it is assumed that quark-antiquark pairs are formed as the result of the decay of a pomeron which has a retardation given by $1/x$. Following this line of reasoning DPM postulates that the retardation of a sea quark or sea antiquark is given by

$$f_{q^{sea}}^{(DPM)}(x) = \frac{1}{\sqrt{x^2 + (\mu^2/s)}} \quad . \quad (4)$$

Where μ is a parameter that sets a mass scale. QGSM postulates, on the other hand, that the retardations of the sea quarks and antiquarks have the same origin as that for valence quarks and, hence, are the same functions. I adopt this latest view in the present work. While there are no practical difference in terms of computational results at ISR energies, I find QGSM structure functions more coherent with the assumption I have made – sea-valence diquark symmetry. The mechanism considered in DPM to postulate the retardation functions, must be included in a treatment of the problem in which we sum over all possible RFT diagrams. For instance, in the case of two inelastic collisions, one term must correspond to a coupling between the hadron and the two cut pomerons mediated by the exchange of a pomeron (DPM) – PPP diagram, another one to the same coupling mediated by the exchange of a reggeon (QGSM) – PRP diagram. The corresponding relative weights for this kind of diagrams are not known and their computation is an open problem. The choice among neglecting one or the other constitutes a model assumption that can only be justified by the phenomenology^[31]. Yet, the eikonal approximation to RFT points that the PPP diagrams constitute the main contribution to high-mass intermediate states and eventually lead to the point-like quarks structure functions, while the PRP type of diagrams are the dominant terms for low-mass intermediate states^[32]. This idea allowed to understand the data from HERA on small- x behaviour of the structure functions^[33].

The PPP coupling does not allow the inclusion of diagrams of type 3(b). The extra sea quark-antiquark pairs, in collisions with more than one cut pomeron, are the result of the decay of an object with vacuum quantum numbers. Therefore, DPM only allows diagrams of type 3(a). This also explains why only valence diquarks contribute to the final state in DIS and hard hadron-hadron collisions. Then, as far as we are interested in the low- p_\perp regime, it seems most reasonable to adhere to QGSM view.

The s-quark, (us) , (ds) and (ss) retardations are given by the following functions, where α_φ is the intercept of the φ trajectory and $\Delta\alpha = \alpha_R(0) - \alpha_\varphi(0)$.

$$\begin{aligned} f_s(x) &= x^{\alpha_\varphi}, \\ f_{us}(x) &= f_{ds}(x) = x^{\alpha_R(0)-2\alpha_N(0)+\Delta\alpha}, \\ f_{ss}(x) &= x^{\alpha_R(0)-2\alpha_N(0)+2\Delta\alpha}. \end{aligned} \quad (5)$$

The corresponding functions for the uu , ud , and dd diquarks, as well as for the u and d quarks are given in equation 3.

The momentum-fraction distribution function in a nucleon, in the case of N cut pomerons, is given by the following expression:

$$\begin{aligned} \varrho^N(x_{i_1}, x_{i_2}, \dots, x_{i_N}, x_{i_d}, x_{\bar{i}_2}, \dots, x_{\bar{i}_N}) &= C_{i_1, i_2, \dots, i_N, i_d, \bar{i}_2, \dots, \bar{i}_N}^N \\ \times f_{i_1}(x_{i_1}) f_{i_2}(x_{i_2}) \dots f_{i_N}(x_{i_N}) f_{i_d}(x_{i_d}) f_{\bar{i}_2}(x_{\bar{i}_2}) \dots f_{\bar{i}_N}(x_{\bar{i}_N}) \\ \times \delta(x_{i_1} + x_{i_2} + \dots + x_{i_N} + x_{i_d} + x_{\bar{i}_2} + \dots + x_{\bar{i}_N} - 1) \end{aligned} \quad (6)$$

This function is perfectly defined if we consider that $f_i(x) = f_i(x)$. The indexes $i_j = \{u, s, d\}$ and $i_{\bar{j}} = \{\bar{u}, \bar{d}, \bar{s}\}$, $i_d = \{(uu), (ud), (dd), (us), (ds), (ss)\}$. Since we are considering nucleons as the colliding particles, the diquark can be of type (ss) only if $N \geq 3$ and of types (us) or (ds) if $N \geq 2$; we find the s-quark retardation only when $N \geq 2$.

The single-parton structure functions are obtained integrating over all other momentum fractions:

$$\begin{aligned} \rho_{u,d}^{(N)}(x) &= C_0^{q,N} x^{-\alpha_R(0)} (1-x)^{\alpha_R(0)-2\alpha_N(0)+(N-1)2(1-\alpha_R(0))} \\ &\quad \times [1 - \gamma + \gamma(1-x)^{2\Delta\alpha}]^{N-1} \\ &= C_0^{q,N} x^{-\frac{1}{2}} (1-x)^N (1-\gamma x)^{N-1}, \quad N \geq 1 \\ \rho_s^{(N)}(x) &= C_1^{q,N} x^{-\alpha_\varphi(0)} (1-x)^{\alpha_R(0)-2\alpha_N(0)+2(N-2)(1-\alpha_R(0))+2-\alpha_R(0)-\alpha_\varphi(0)} \\ &\quad \times [1 - \gamma + \gamma(1-x)^{2\Delta\alpha}]^{N-2} \\ &= C_1^{q,N} (1-x)^{N+\frac{1}{2}} (1-\gamma x)^{N-2}, \quad N \geq 2 \\ \rho_{uu,ud,dd}^{(N)}(x) &= C_0^{qq,N} x^{\alpha_R(0)-2\alpha_N(0)} (1-x)^{-\alpha_R(0)+2(N-1)(1-\alpha_R(0))} \\ &\quad \times [1 - \gamma + \gamma(1-x)^{2\Delta\alpha}]^{N-1} \\ &= C_0^{qq,N} x (1-x)^{N-\frac{3}{2}} (1-\gamma x)^{N-1}, \quad N \geq 1 \\ \rho_{us,ds}^{(N)}(x) &= C_1^{qq,N} x^{\alpha_R(0)-2\alpha_N(0)+\Delta\alpha} (1-x)^{-\alpha_\varphi(0)+2(N-1)(1-\alpha_R(0))} \end{aligned} \quad (7)$$

$$\begin{aligned} & \times [1 - \gamma + \gamma(1 - x)^{2\Delta\alpha}]^{N-2} \\ &= C_1^{qq,N} x^{\frac{3}{2}} (1 - x)^{N-1} (1 - \gamma x)^{N-2}, \quad N \geq 2 \end{aligned} .$$

$$\begin{aligned} \rho_{ss}^{(N)}(x) &= C_2^{qq,N} x^{\alpha_R(0) - 2\alpha_N(0) + 2\Delta\alpha} (1 - x)^{-\alpha_R(0) + 2(N-2)(1 - \alpha_R(0)) + 2(1 - \alpha_\varphi(0))} \\ & \times [1 - \gamma + \gamma(1 - x)^{2\Delta\alpha}]^{N-3} \\ &= C_2^{qq,N} x^2 (1 - x)^{N-\frac{1}{2}} (1 - \gamma x)^{N-3}, \quad N \geq 3 \end{aligned} .$$

The numerical values for the constants are $\alpha_R(0) = 0.5$, $\Delta\alpha = 0.5$ and $\alpha_N = -0.25$. The value of α_N has been chosen within the theoretically allowed range to obtain the best agreement with the proton-proton data.

The factors $[1 - \gamma + \gamma(1 - x)^{2\Delta\alpha}]^{N-J}$ in equation (7) have their origin in the fact that the s quarks take a larger portion of the nucleon momentum than the u or d quarks. It has a little effect on the structure functions when N is small. When N is large, these factors make the functions steeper at $x \rightarrow 0$.

2.2 Fragmentation Functions

The fragmentation functions are derived from Regge arguments^[34, 35]. The ones needed for the present work are listed in the appendix. I have corrected some missprints in ref. [35] and use consistently the value of α_N given above³. The constant $\lambda = 2\alpha' \bar{p}_\perp^2 \simeq 0.5$, where α' is the slope of the Regge trajectory, has been used in the expressions.

All these functions are proportional to one of the constants a_p , a_Λ , $a_{\bar{p}}$ and $a_{\bar{\Lambda}}$, which represent the universal rapidity densities of protons, Λ hyperons, antiprotons and anti- Λ hyperons respectively, around the centre-of-mass of the string. The fragmentation of a diquark into a given baryon contains two terms, one corresponds to the creation of a hadron that contains the baryon number of the diquark: primary or leading fragmentation (subindex 1), the other comes from baryon-antibaryon formation in the string: secondary fragmentation (subindex 2). Hence, the latest is proportional to the corresponding antibaryon density. Functions such as $D_{1,uu}^p(z)$, include a factor function linear with z . This is introduced to take into account the excess in the production of baryons containing the whole diquark over those that contain only one of the quarks of the diquark. Taking into account the constants that define these factors, c_0 , c_1 and c_2 , we have seven parameters with only three of them independent. This is so because I assume that the baryon number sum rule saturates with protons, neutrons and Λ hyperons. This is a sensible approximation since other stable baryons contribute to the final state in a much smaller proportion⁴.

As we also need the fragmentation functions for diquarks with strangeness -1 and -2 , they were obtained applying the results of ref. [34]. I have assumed that both strange and non-strange quarks are dynamically symmetric, hence the factor $(1 + \sqrt{z})/2$. The fragmentation of a diquark into a baryon that do not contain any quark from the diquark is taken to be 0. This may be controversial since it has been suggested^[32] that an excess in the production of

³The treatment of the fragmentation functions in ref. [10] is inconsistent since two different values for α_N , -0.25 and -0.5 , were used simultaneously. This second value was also used to compute the structure functions.

⁴In ref. [10] the constraint imposed by baryon number conservation was overlooked and different values for the baryon densities in the strings were used.

Ω^- over Ω^+ , in non-strange hadrons collisions, contradicts this assumption. As a matter of fact, preliminary data show a very small asymmetry in π -nucleus interactions at 500GeV/c^{36]}. Nevertheless, although the data are still inconclusive, this effect, if small as it seems, may be understood in the framework of the model described in this paper: multiple collision raises the probability of having contributions to the final state coming from the fragmentation of strange diquarks that results in a net production of Ω^- .

2.3 Rapidity Distributions

We concentrate in the study of collisions between identical nuclei. The atomic weight and the atomic number are A and Z respectively. The rapidity distribution for the production of a hadron h is given by:

$$\frac{dN_{AB}^{(h)}}{dy} = \frac{1}{\sigma_{AB}} \sum_{(n_A, n_B, n, \mu_A, \mu_B)} \sigma^{n_A, n_B, n, \mu_A, \mu_B} \{ \theta(n_B - n_A) [n_A (N_{\mu_A \mu_B}^{q q^A - q^B}(y) + N_{\mu_A \mu_B}^{q^A - q q^B}(y)) + (n_B - n_A) (N_{\mu_A \mu_B}^{\bar{q}^A - q^B}(y) + N_{\mu_A \mu_B}^{q^A - \bar{q}^B}(y)) + (n - n_B) (N_{\mu_A \mu_B}^{q^A - \bar{q}^B}(y) + N_{\mu_A \mu_B}^{\bar{q}^A - q^B}(y))] + \text{Symmetric terms}(n_A \leftrightarrow n_B) \} . \quad (8)$$

In writing this expression, I neglect kinematical correlations among different strings, $N_{\mu_A \mu_B}^{a-b}$. Here, $\sigma^{n_A, n_B, n, \mu_A, \mu_B}$ is the cross-section for AB collisions where there are n inelastic nucleon-nucleon collisions involving n_A nucleons of A and n_B nucleons of B , in which at least one of the participating nucleons of A (B) suffers μ_A (μ_B) inelastic collisions.

I restrict the discussion to the case $A = B$. We can approximate equation 8, with a good degree of accuracy using average values for n_A , n_B and n .

$$\frac{dN_{AB}^{(h)}}{dy} = \bar{n}_A (N_{\bar{\mu}_A \bar{\mu}_A}^{q q^A - q^B}(y) + N_{\bar{\mu}_A \bar{\mu}_A}^{q^A - q q^B}(y)) + (\bar{n} - \bar{n}_B) (N_{\bar{\mu}_A \bar{\mu}_A}^{q^A - \bar{q}^B}(y) + N_{\bar{\mu}_A \bar{\mu}_A}^{\bar{q}^A - q^B}(y)) . \quad (9)$$

Equation (9) is obtained by neglecting the dependence of the string density N on the μ 's, which are replaced by their average values $\bar{\mu}$ ⁵.

$$N_{\mu_1, \mu_2}^{a-b}(y) = \sum_{i,j} w_N^i w_N^j \int_0^1 \int_0^1 dx_1 dx_2 \varrho_{\mu_1}^{a_i}(x_1) \varrho_{\mu_2}^{b_j}(x_2) \frac{dN^{a_i-b_j}}{dy}(y - \Delta, s_h^{a_i-b_j}) \theta(sx_1 x_2 - s_h^{a_i-b_j}) . \quad (10)$$

Here a and b refer to quark or diquark. A sum is performed over all possible partons flavours i and j . The probability weights w^i and w^j are trivially computed from the model assumptions. They depend on γ , A and Z . A mass threshold for each chain is enforced by the θ -function. Please note that this mass threshold is not always equal to the mass of hadron h since the flavour structure of the string many times forces to have other hadrons besides h in the final state. Δ is the center-of-mass rapidity of the string.

⁵In practical computations a slightly more accurate expression has been used in which the average of densities over $\mu_B = \mu_A$ were taken using the weights $\sigma_{NA}^{\mu_A}/\sigma_{NA}$. These weights are obtained from ref. [37]. No significant numerical difference were observed compared to the results obtained using $\bar{\mu}_A \simeq \bar{n}/\bar{n}_A$.

$$\frac{dN^{a_i-b_j}}{dy}(y - \Delta, s_h^{a_i-b_j}) = \begin{cases} G_{a_i}^h(y) & \text{if } y \geq \Delta \\ G_{b_j}^h(y) & \text{if } y \leq \Delta \end{cases}, \quad (11)$$

where $G(y)$ are the fragmentation functions:

$$\begin{aligned} G_{a_i}^h(y) &= Z_+ D_{a_i}^h(Z_+) \\ G_{b_j}^h(y) &= Z_- D_{b_j}^h(Z_-) \end{aligned}, \quad (12)$$

Here $Z_+ = \exp[(y - \Delta) - y_{MAX}]$ and $Z_- = \exp[-(y - \Delta) - y_{MAX}]$, y_{MAX} being the maximum rapidity that hadron h can have in the string for fixed values of momentum fractions x_1 and x_2 .

3 Proton-proton collisions

Since I have not considered sum rules others than the ones due to baryon conservation, the model leaves three free parameters that I have fixed in order to obtain the best fits to proton-proton data. At ISR energies, the structure of these collisions is very simple: we only need to consider one pomeron exchange. Therefore, the only differences between the results of the present model and those from DPM and QGSM, at this stage, come from the choice of α_N , that was usually taken in the past to be near -0.5 .

Figure 4 represents the Feynman x distribution of protons produced in the reaction $pp \rightarrow pX$. The fit obtained agrees very well with the experimental data taken from ref. [38] particularly in the region $x_F < 0.75$. It has been pointed out that experimental points above that cut are not very reliable (see [38]) due to detector inefficiencies. The fit in the region $x \rightarrow 0$ is very sensitive to the value of α_N . For $\alpha_N = -0.5$ the results of the fit are much poorer than the one shown, which corresponds to the value of $\alpha_N = -0.25$ consistently used throughout this paper. The value of a_p fixes the values of the remaining parameters by the use of the sum rules. Figure 5 shows the fit to $pp \rightarrow \bar{p}X$. It is also worth mentioning that the same value for $a_{\bar{p}}$ was independently obtained from both fits.

To obtain the value of $a_{\bar{\Lambda}}$, I used the data from ref. [39] that were taken at a similar centre-of-mass energy. The reactions considered are $pp \rightarrow \Lambda X$ and $pp \rightarrow \bar{\Lambda} X$. We show the best fits in figures 6 and 7 (please mind that in this two fits only $a_{\bar{\Lambda}}$ is free, since a_{Λ} is given by the sum rules and the value of a_p). The large error bars in the experimental data do not allow for a very accurate determination of $a_{\bar{\Lambda}}$. I have taken the value that best fits the data and also that is compatible with a mass suppression factor of introduced in [34].

The numerical values obtained are: $a_p = 0.667$, $a_{\Lambda} = 0.282$, $a_{\bar{p}} = 0.077$, $a_{\bar{\Lambda}} = 0.045$, $c_0 = 1.430$, $c_1 = 6.076$ and $c_2 = 67.560$.

4 Nucleus-Nucleus collisions

At this point we have a model for nucleus-nucleus collisions which contains no free parameters.

The result for the rapidity distribution of Λ hyperons produced in central sulfur-sulfur collisions is compared with the experimental data from the CERN-NA35^[11] collaboration in figure 8. The dashed line corresponds to the results of the model without the sea-valence

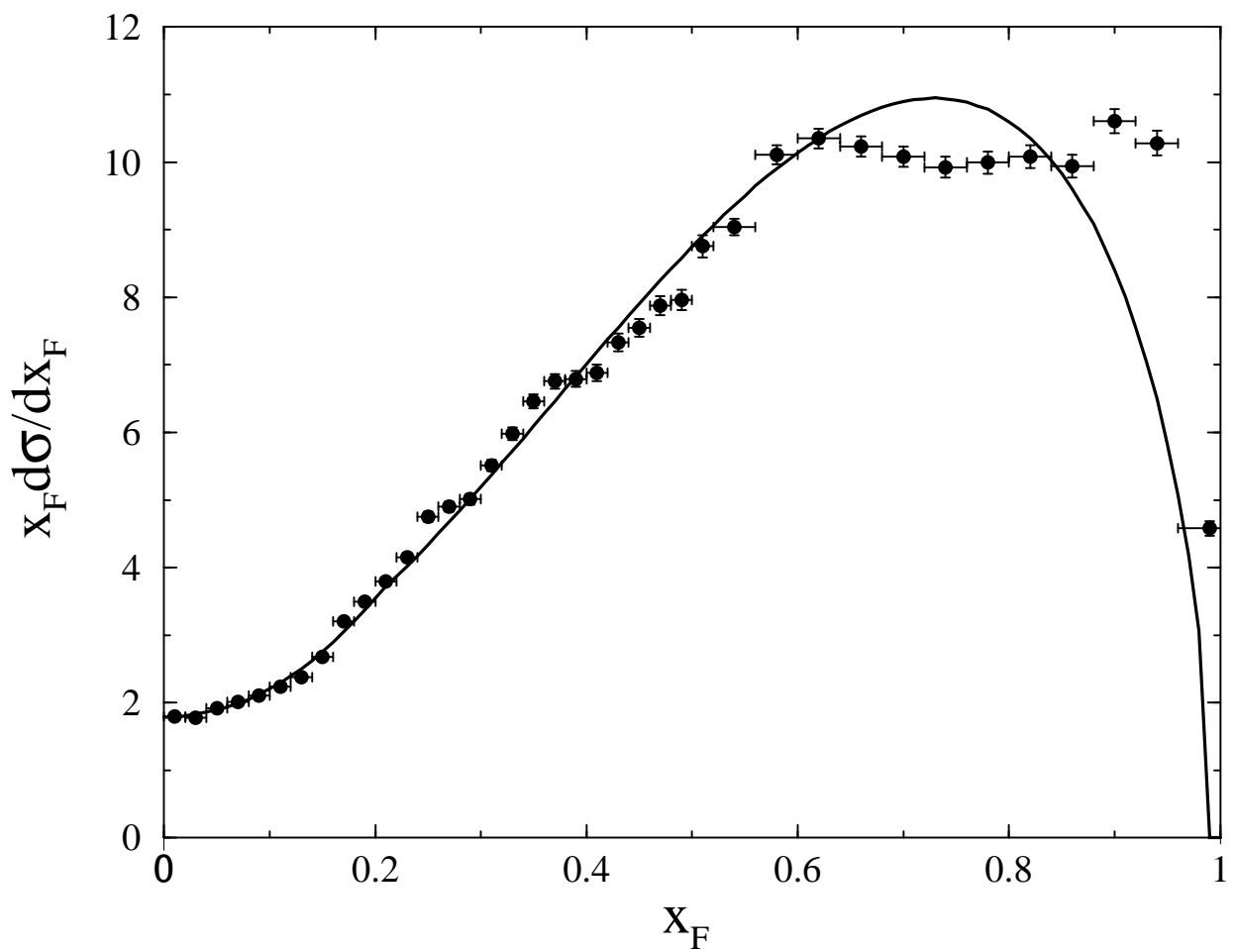


Figure 4: Fit to the Feynman x distribution of protons in the reaction $pp \rightarrow pX$. Data correspond to $p_{\text{lab}} = 400$ GeV and were taken from ref. [38].

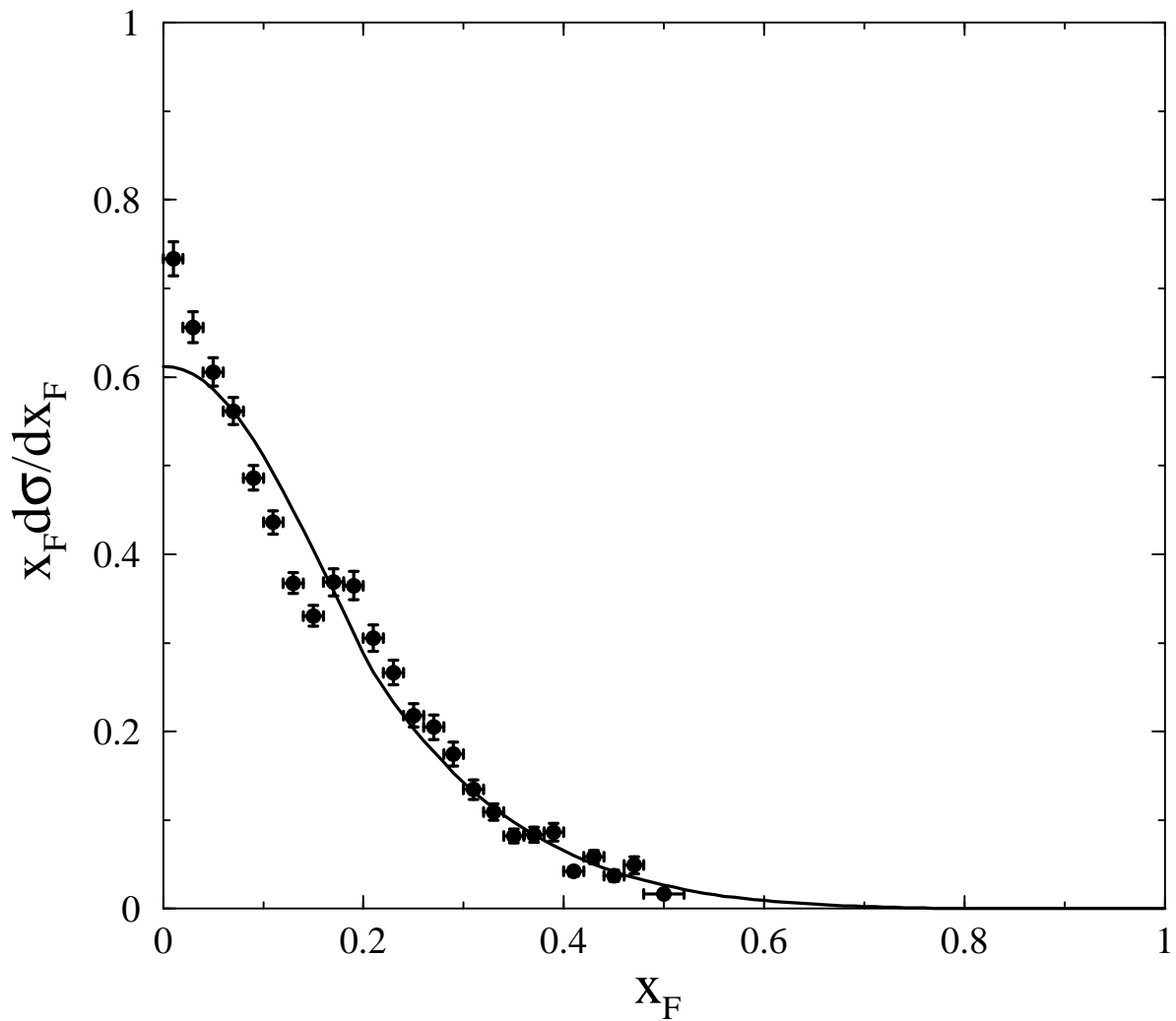


Figure 5: Fit to the Feynman x distribution of antiprotons produced in the reaction $pp \rightarrow \bar{p}X$. Data correspond to $p_{\text{lab}} = 400$ GeV and were taken from ref. [38].

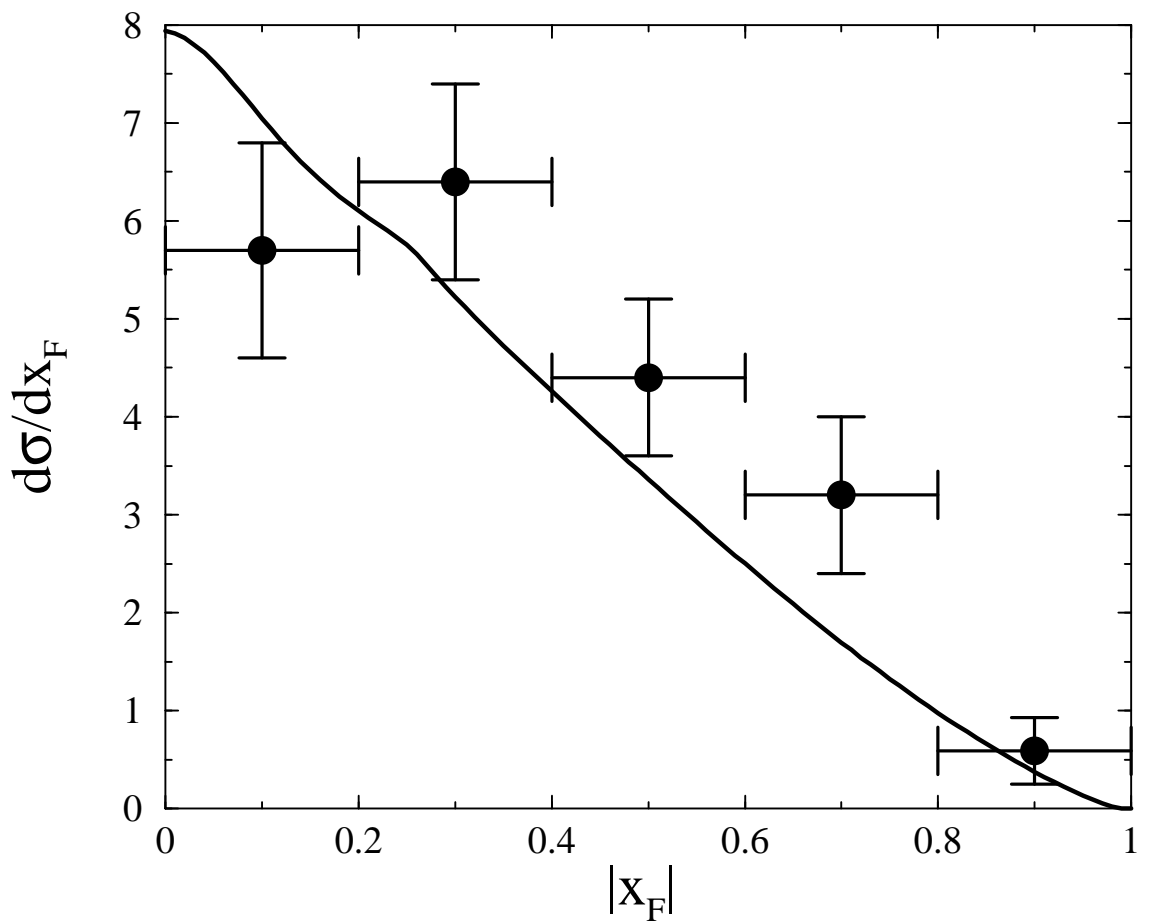


Figure 6: Fit to the Feynman x differential cross section $d\sigma/dx$ (given in mb) for the inclusive production of Λ in the reaction $pp \rightarrow \Lambda X$. Data correspond to $p_{\text{lab}} = 405$ GeV and were taken from ref. [39].

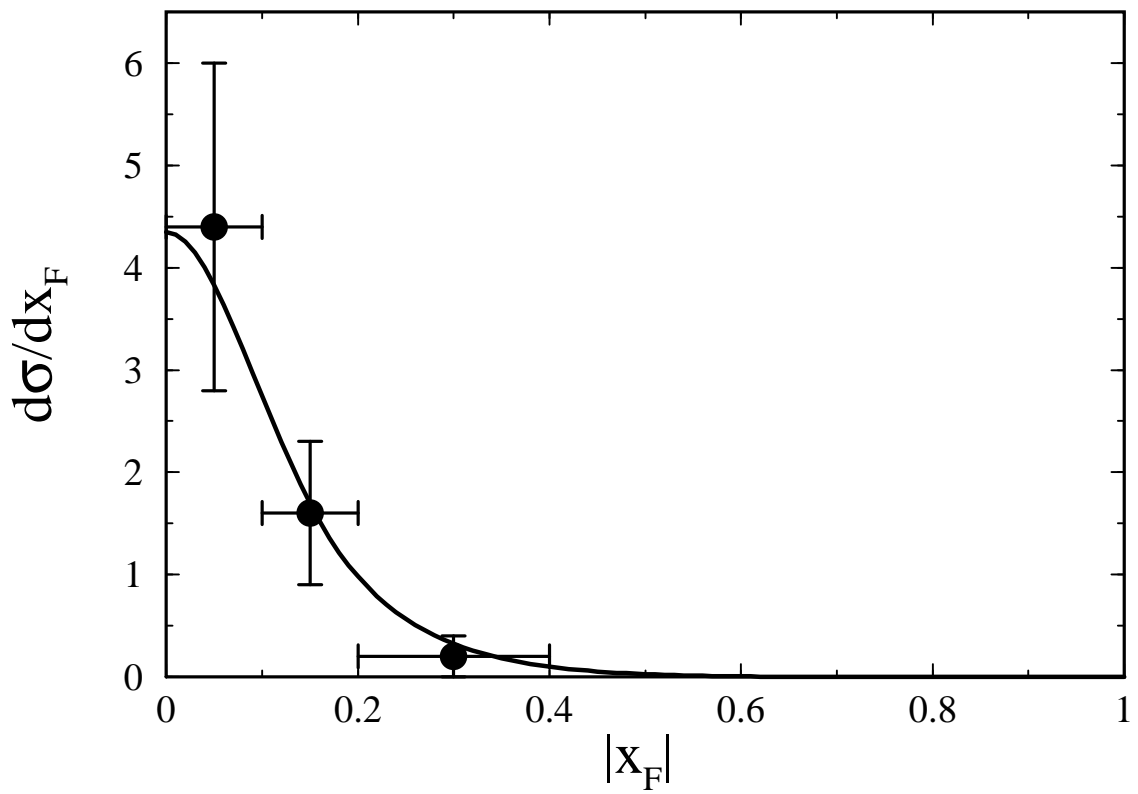


Figure 7: Fit to the Feynman x differential cross section $d\sigma/dx$ (given in mb) for the inclusive production of $\bar{\Lambda}$ in the reaction $pp \rightarrow \bar{\Lambda}X$. Data correspond to $p_{\text{lab}} = 405$ GeV and were taken from ref. [39].

diquark symmetry introduced in this paper. As we can see, both models give similar results at $y_{CM} = 0$, while there is a remarkable difference in the fragmentation region where only the present model reproduces the data. The data are not corrected for particles originated from electromagnetic Σ^0 ($\bar{\Sigma}^0$) decays and from weak Ξ ($\bar{\Xi}$) decay. These decays have not been included in the model. Figure 9 shows the agreement between the $\bar{\Lambda}$ distribution and the data points from the same experiment. The only disagreement is with the point near $y_{CM} = 0$ in the Λ distribution. I will comment on this in the conclusions.

Figure 10 shows the proton minus antiproton distribution in central (solid line) and peripheral (dashed-dotted line) sulfur-sulfur collisions. The data points were also taken by the CERN-NA35 collaboration^[12]. For central collisions, the agreement in the fragmentation region of the spectrum is very good while the data show an overpopulation of protons around $y_{CM} = 0$. Again, we need to carefully look at the data and stress that what has really been measured is the difference between positively and negatively charged hadrons. The authors claim that, due to secondary $p - \bar{p}$ and $\pi^+ - \pi^-$ cancellations (the difference $K^+ - K^-$ has been estimated using a Monte Carlo simulation), this corresponds to the primary proton distribution. While this cancellations must be true for overall secondary baryon-antibaryon production, there is no reason to believe that the secondary proton spectrum is exactly equal to the antiproton spectrum. But, what is more important to understand the central rapidity region is that an excess of π^+ mesons over π^- has been observed in proton-proton collisions^[38]. This difference is due, in the fragmentation region, to the excess of u quarks over d quarks in a proton-proton collision. On the other hand, it is a well established fact that the composition of the central rapidity region is independent of the quark content of the colliding hadrons, so must be this asymmetry. We can use the approximate scaling of the pions distribution at $y_{CM} = 0$ with the number of participating nucleons of one nucleus, \bar{n}_A , to estimate the excess of positive charge. Please mind that this estimate is very inaccurate away from this region as it quickly decreases for larger values of y_{CM} due to the isospin symmetry of sulphur nuclei. The corresponding correction is shown in the graph with a small dotted line. As it can be appreciated, once taking this correction into account the experimental data are perfectly understood.

Finally, figure 11 shows the predictions for the rapidity spectra of primary protons, Λ and $\bar{\Lambda}$ produced in central Pb-Pb collisions.

As mentioned before, I have made use of the Galuber-Gribov model to obtain the average numbers of participating nucleons and nucleon-nucleon collisions. I have used the value $\sigma_{NN}^{\text{in}} = 30$ mb for the inelastic nucleon-nucleon cross section. The profile functions were obtained using the nuclear matter distribution given in ref. [40]. They consist of three parameters, individually fitted to nuclear data, and are more accurate than the Saxon-Wood density functions used in the past. The actual numerical values used for central S-S, $\bar{n}_A = 27.8$ and $\bar{n} = 62.8$, were obtained requiring that $b < 1$, where b is the impact parameter. For peripheral collisions we have $\bar{n}_A = 9.7$ and $\bar{n} = 14.7$, while for central Pb-Pb collisions are $\bar{n}_A = 204.4$ and $\bar{n} = 895.9$.

To perform the computations, I have taken the values of the proton and Λ transverse mass equal to 1.1 and 1.3 GeV respectively, in agreement with the data from [15].

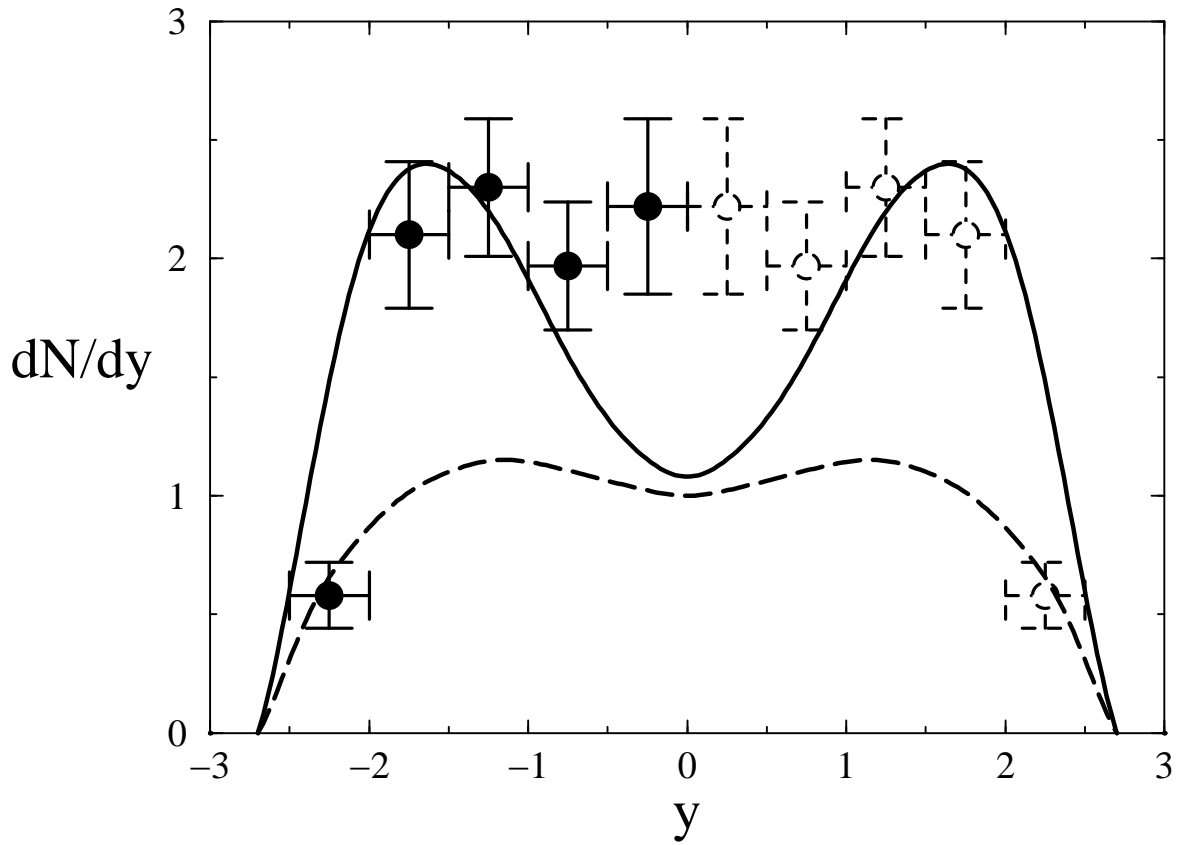


Figure 8: Rapidity distribution of Λ 's produced in central sulphur-sulphur collisions represented in the nucleon-nucleon centre-of -mass reference frame. The solid line correspond to the results of this model while the dashed line are the results obtained when the new components are not included. The data points are from ref.[11] and have been reflected onto positive rapidities.

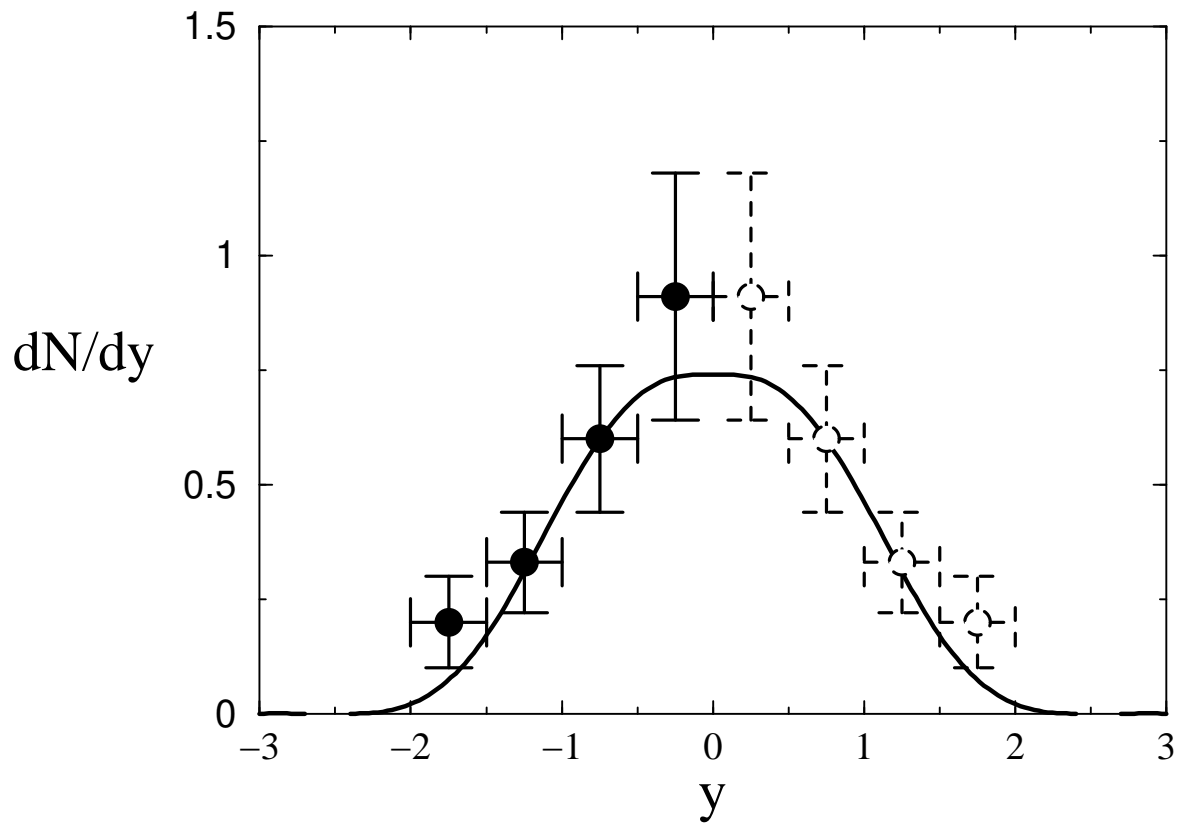


Figure 9: Rapidity distribution of $\bar{\Lambda}$'s produced in central sulphur-sulphur collisions represented in the nucleon-nucleon centre-of-mass reference frame. The data points are from ref. [11] and have been reflected onto positive rapidities.

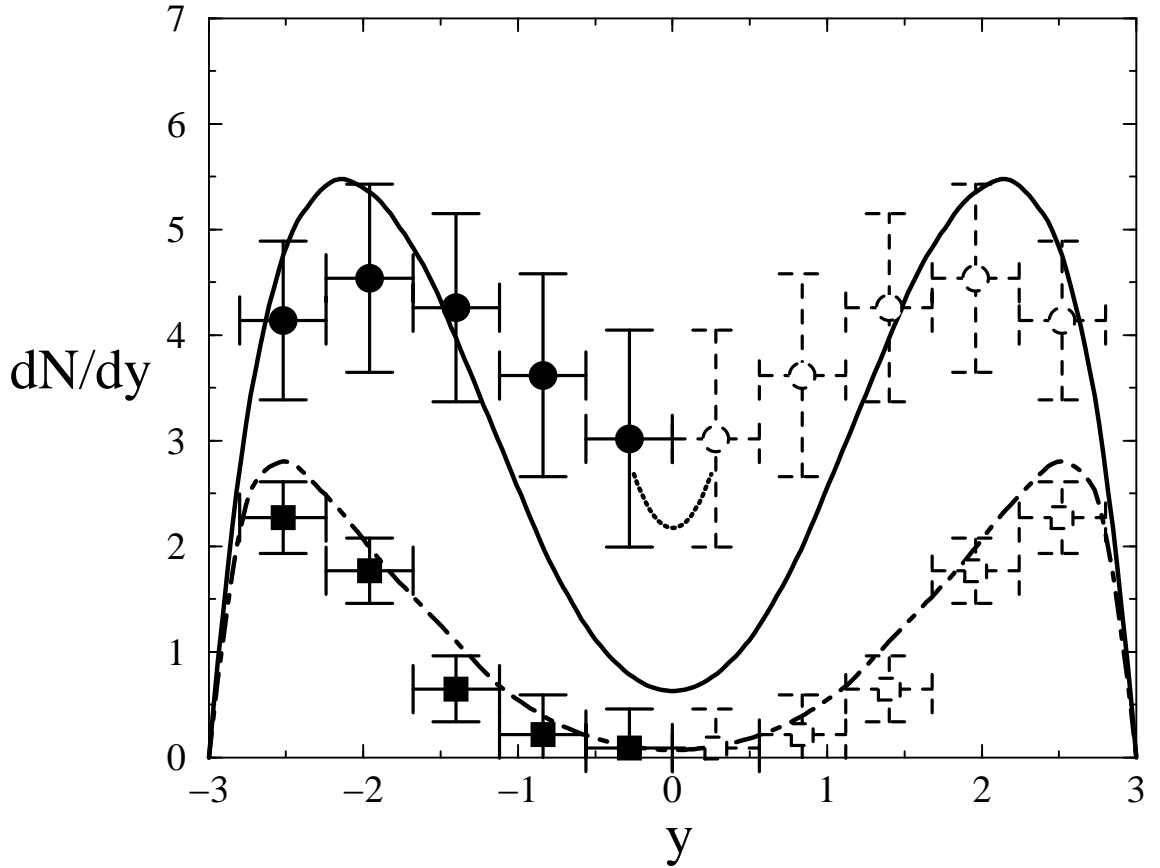


Figure 10: Rapidity distribution of protons produced in sulphur-sulphur collisions represented in the nucleon-nucleon centre-of-mass reference frame. The dashed-dotted line corresponds to primary protons produced in peripheral collisions; the solid line are the results for the proton minus antiproton distribution in central collisions. The data points are from ref. [12] and have been reflected onto positive rapidities. The small dotted line represent the results for central collisions corrected with the $\pi^+ - \pi^-$ asymmetry experimentally observed. See text for a more detailed explanation.

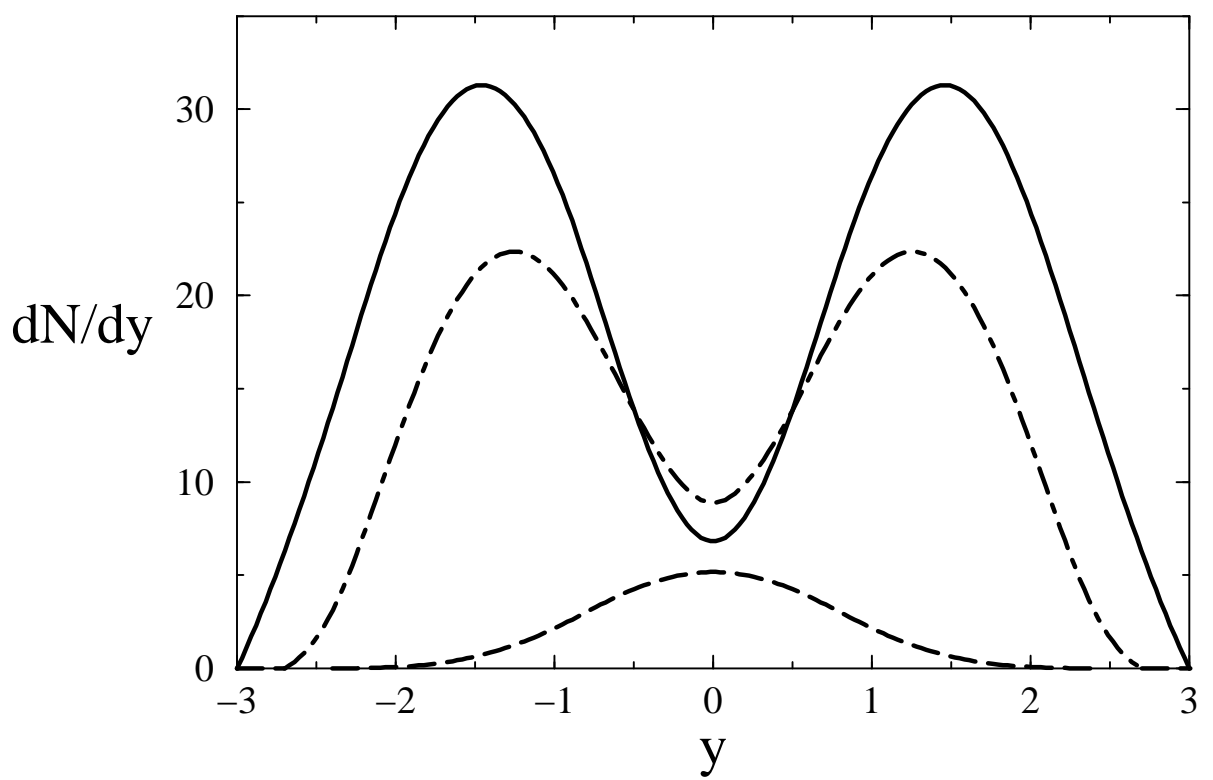


Figure 11: Rapidity distribution of primary protons (solid line), Λ 's (dashed-dotted line) and $\bar{\Lambda}$'s (dashed line) produced in central Pb Pb collisions represented in the nucleon-nucleon centre-of-mass reference frame.

5 Conclusions

In order to explain the data on baryon rapidity spectra presented by the NA35 collaboration, I have included into the DPM and the QGSM models components that were previously overlooked. They are compatible with the $1/N$ expansion of QCD on which these two models are based. A discussion over the right structure functions for the string's ends leads to the adoption of the ones proposed by the QGSM, as they are the only ones consistent with the model's assumptions. The fragmentation functions are obtained from the planar approximation to Regge diagrams. They have been published elsewhere except for the ones corresponding to strange diquark that are published here for the first time. All of them are given in the appendix. Once taken into account the baryon-number sum-rules, the number of free parameters of the model is reduced to 3. The numerical values of these parameters have been obtained fitting data of inclusive baryon and antibaryon production in proton-proton collisions. The sum rules allow us to obtain the fragmentation functions that do not contribute to proton-proton collisions at ISR energies.

The model has strong theoretical grounds and all the approximations done are well justified, being the uncertainties introduced by them small and well under control.

At the level of nucleus-nucleus collisions, we have a model which contains no free parameters. The $\bar{\Lambda}$ distribution for central sulphur-sulphur collisions was computed and a perfect agreement with the experimental data was obtained. This result does not depend on the new components introduced in this paper; all the $\bar{\Lambda}$ particles come from baryon-antibaryon formation in the strings, which is essentially independent of the parton components at the end of the string. This result is very relevant since it clearly shows that the \bar{s} content at the central rapidity region is very well understood with no need to assume collective effects such as QGP formation.

I have also computed the rapidity distribution for the Λ hyperons for central sulphur-sulphur collisions and compared it with data from the same collaboration. The results show a remarkable increase of the rapidity distribution in the fragmentation region well in agreement with the experimental data. This is due to the inclusion of chains initiated by diquarks that can contain a quark from the nucleon sea. The fact that this sea-quark has a probability of being a strange quark, obtained by independent analysis, is responsible for this effect. The only disagreement with the data is seen at the central rapidity region. Below I will try to point out the origin of this discrepancy.

The net proton distribution for the same collisions has also been computed and compared with data of the same collaboration published in 1991. The agreement observed with the data is very good. Especially so if we take into account that the distribution published by the NA35 collaboration actually corresponds to the net charge distribution which only coincides with the net proton distribution in the fragmentation region. As a matter of fact, data published on inclusive meson production in 1992 shows a charge asymmetry in the pion sector. This asymmetry is very easily understood since it is needed to ensure total charge conservation. The positive charge lost by the production of primary Λ hyperons at the expense of protons and neutrons can only be compensated by a charge excess in the meson sector where baryon number conservation do not apply. The extrapolation of this asymmetry at $y_{CM} = 0$ to the nucleus-nucleus collisions, using the observed approximate scaling at $y_{CM} = 0$ with the number of wounded nucleons of a nucleus, perfectly reproduces the data point in this region. We can also conclude that the models that have been proposed to reproduce the NA35 data on net

charge distribution taking them as the true net proton distribution are misguided.

We come back now to the discussion of the only point with which the Λ distribution do not agree. Corrections had to be applied to obtain that point based on Monte Carlo simulation. It can not be otherwise due to the large multiplicities of secondaries in these events. It is very possible that the Monte Carlo simulations were adjusted to reproduce the data of the wrong proton distribution giving as a result an overestimation of the correction applied to this experimental point. Until we do not have a more detailed information on how the analysis was done, these are only speculations but they are grounded on one fact. Once we understand the net proton distribution, there are no rational explanations left to make sense of this experimental point as it is clear that the extra hyperons allegedly observed should be primary baryons. The formation of QGP would never produce net baryon charge. Other mechanism such as sea quark-antiquark formation face the same problem. As for the effects due to final state interactions, we clearly see that, allowing interactions among comovers, i. e. among particles with similar rapidities, even under the unreasonable assumption that all the protons in the central region would turn into Λ , we would not be able to reproduce this controversial experimental point.

The NA35 data on baryon distributions do not support that the formation of QGP has taken place. It is nevertheless possible that the forthcoming data from PbPb will show that the necessary condition for that phase transition have been attained. I have also presented the model predictions for this experiment. Although it is necessary to take the data in the central rapidity region with due care as the experimental analyses of that region are extremely complicated and many corrections, some times model dependent, have to be applied.

An other important conclusion, that has been obtained as a byproduct, is that the analysis performed on the proton-proton data strongly support a value for the intercept of the N trajectory close to -0.25 . This is also a major result of the model that in return can help to establish a more accurate value for the mass of some resonances.

For future works it is left the detailed study of the meson sector. Also the implications of the new structure of the pomeron-hadron coupling discussed in the paper will be investigated in order to shed light on other outstanding problems such as heavy quark formation in hadronic and nuclear collisions.

Acknowledgements. I want to thank A. Capella for his continuous support and encouragement, also for pointing out a mistake in the first version of the manuscript. To him and to A. Kaidalov for discussions and many useful explanations and comments about their previous works. Also my gratitude goes to N. Armesto, S. Pepin and M. McDermott for comments and discussions and to A. Sabio-Vera for help with the technicalities of typesetting the manuscript.

Appendix

I list here the fragmentation functions into baryons and antibaryons. The ones not shown can be obtained applying isospin symmetry $p \leftrightarrow n$, $u \leftrightarrow d$.

$$\begin{aligned}
D_{1,uu}^p &= \frac{a_p}{z} z^{2(\alpha_R(0)-\alpha_N(0))} (1-z)^{-\alpha_R(0)+\lambda} (1+c_0z) = \frac{a_p}{z} z^{1.5} (1+c_0z) \\
D_{1,uu}^n &= \frac{2}{3} \frac{a_p}{z} z^{2(\alpha_R(0)-\alpha_N(0))} (1-z)^{-\alpha_R(0)+\lambda+2(1-\alpha_R(0))} = \frac{2}{3} \frac{a_p}{z} z^{1.5} (1-z) \\
D_{1,uu}^\Lambda &= \frac{a_\Lambda}{z} z^{2(\alpha_R(0)-\alpha_N(0))} (1-z)^{-\alpha_R(0)+\lambda+\Delta\alpha+2(1-\alpha_R(0))} = \frac{a_\Lambda}{z} z^{1.5} (1-z)^{1.5} \\
D_{1,ud}^p &= \frac{a_p}{z} z^{2(\alpha_R(0)-\alpha_N(0))} (1-z)^{-\alpha_R(0)+\lambda} = \frac{a_p}{z} z^{1.5} = D_{1,ud}^n \\
D_{1,ud}^\Lambda &= \frac{a_\Lambda}{z} z^{2(\alpha_R(0)-\alpha_N(0))} (1-z)^{-\alpha_R(0)+\Delta\alpha+\lambda} = \frac{a_\Lambda}{z} z^{1.5} (1-z)^{0.5} \\
D_{1,dd}^p &= D_{1,uu}^n \quad , \quad D_{1,dd}^n = D_{1,uu}^p \quad , \quad D_{1,dd}^\Lambda = D_{1,uu}^\Lambda \\
D_{1,us}^p &= \frac{1}{2} \frac{a_p}{z} z^{2(\alpha_R(0)-\alpha_N(0))} (1-z)^{-\alpha_R(0)+\lambda+\Delta\alpha+2(1-\alpha_R(0))} (1+z^{\Delta\alpha}) = D_{1,us}^n \\
&= \frac{1}{2} \frac{a_p}{z} z^{1.5} (1-z)^{1.5} (1+z^{\frac{1}{2}}) \\
D_{1,us}^\Lambda &= \frac{1}{2} \frac{a_\Lambda}{z} z^{2(\alpha_R(0)-\alpha_N(0))} (1-z)^{-\alpha_R(0)+\lambda} (1+z^{\Delta\alpha}) (1+c_1z) \\
&= \frac{1}{2} \frac{a_\Lambda}{z} z^{1.5} (1+z^{\frac{1}{2}}) (1+c_1z) \\
D_{1,ds}^p &= D_{1,us}^p \quad , \quad D_{1,ds}^n = D_{1,us}^n \quad , \quad D_{1,ds}^\Lambda = D_{1,us}^\Lambda \quad , \quad D_{1,ss}^p = 0 \quad , \quad D_{1,ss}^n = 0 \\
D_{1,ss}^\Lambda &= \frac{a_\Lambda}{z} z^{2(\alpha_R(0)-\alpha_N(0))+\Delta\alpha} (1-z)^{-\alpha_R(0)+\lambda+\Delta\alpha+2(1-\alpha_R(0))} (1+c_2z) \\
&= \frac{a_\Lambda}{z} z^2 (1-z)^2 (1+c_2z) \\
D_{2,uu}^{p,n} &= D_{2,ud}^{p,n} = D_{2,dd}^{p,n} = \frac{a_{\bar{p}}}{z} (1-z)^{-\alpha_R(0)+\lambda+4(1-\alpha_N(0))} = \frac{a_{\bar{p}}}{z} (1-z)^5 \\
D_{2,uu}^\Lambda &= D_{2,ud}^\Lambda = D_{2,dd}^\Lambda = \frac{a_{\bar{\Lambda}}}{z} (1-z)^{-\alpha_R(0)+\lambda+\Delta\alpha+4(1-\alpha_N(0))} = \frac{a_{\bar{\Lambda}}}{z} (1-z)^{5.5} \\
D_{2,us}^{p,n} &= D_{2,ds}^{p,n} np = \frac{a_{\bar{p}}}{z} (1-z)^{-\alpha_R(0)+\lambda+\Delta\alpha+4(1-\alpha_N(0))} = \frac{a_{\bar{p}}}{z} (1-z)^{5.5} \\
D_{2,us}^\Lambda &= D_{2,ds}^\Lambda = \frac{a_{\bar{\Lambda}}}{z} (1-z)^{-\alpha_R(0)+\lambda+2\Delta\alpha+4(1-\alpha_N(0))} = \frac{a_{\bar{\Lambda}}}{z} (1-z)^6 \\
D_{2,ss}^{p,n} &= \frac{a_{\bar{p}}}{z} (1-z)^{-\alpha_R(0)+\lambda+2\Delta\alpha+4(1-\alpha_N(0))} = \frac{a_{\bar{p}}}{z} (1-z)^6 \\
D_{2,ss}^\Lambda &= \frac{a_{\bar{\Lambda}}}{z} (1-z)^{-\alpha_R(0)+\lambda+3\Delta\alpha+4(1-\alpha_N(0))} = \frac{a_{\bar{\Lambda}}}{z} (1-z)^{6.5} \\
D_u^p &= D_d^n = \frac{a_{\bar{p}}}{z} (1-z)^{\alpha_R(0)-2\alpha_N(0)+\lambda} = \frac{a_{\bar{p}}}{z} (1-z)^{1.5} \\
D_u^\Lambda &= D_d^\Lambda = \frac{a_{\bar{\Lambda}}}{z} (1-z)^{\alpha_R(0)-2\alpha_N(0)+\lambda+\Delta\alpha} = \frac{a_{\bar{\Lambda}}}{z} (1-z)^2 \\
D_d^p &= D_u^n = \frac{a_{\bar{p}}}{z} (1-z)^{\alpha_R(0)-2\alpha_N(0)+\lambda} \left(\frac{1}{3} + \frac{2}{3} (1-z) \right) = \frac{a_{\bar{p}}}{z} (1-z)^{1.5} \left(\frac{1}{3} + \frac{2}{3} (1-z) \right) \\
D_s^{p,n} &= \frac{a_{\bar{p}}}{z} (1-z)^{\alpha_R(0)-2\alpha_N(0)+\lambda+2(1-\alpha_R(0))+\Delta\alpha} = \frac{a_{\bar{p}}}{z} (1-z)^3 \\
D_s^\Lambda &= \frac{a_{\bar{\Lambda}}}{z} (1-z)^{\alpha_R(0)-2\alpha_N(0)+\lambda} = \frac{a_{\bar{\Lambda}}}{z} (1-z)^{1.5} \\
D_{uu}^{\bar{p},\bar{n}} &= D_{ud}^{\bar{p},\bar{n}} = D_{dd}^{\bar{p},\bar{n}} = \frac{a_{\bar{p}}}{z} (1-z)^{\alpha_R(0)-2\alpha_N(0)+\lambda+2(1-\alpha_N(0))} = \frac{a_{\bar{p}}}{z} (1-z)^4
\end{aligned}$$

$$\begin{aligned}
D_{uu}^{\bar{\Lambda}} &= D_{ud}^{\bar{\Lambda}} = D_{dd}^{\bar{\Lambda}} = \frac{a_{\bar{\Lambda}}}{z} (1-z)^{\alpha_R(0)-2\alpha_N(0)+\lambda+\Delta\alpha+2(1-\alpha_N(0))} = \frac{a_{\bar{\Lambda}}}{z} (1-z)^{4.5} \\
D_{us}^{\bar{p},\bar{n}} &= D_{ds}^{\bar{p},\bar{n}} = \frac{a_{\bar{p}}}{z} (1-z)^{\alpha_R(0)-2\alpha_N(0)+\lambda+\Delta\alpha+2(1-\alpha_N(0))} = \frac{a_{\bar{p}}}{z} (1-z)^{4.5} \\
D_{us}^{\bar{\Lambda}} &= D_{ds}^{\bar{\Lambda}} = \frac{a_{\bar{\Lambda}}}{z} (1-z)^{\alpha_R(0)-2\alpha_N(0)+\lambda+2\Delta\alpha+2(1-\alpha_N(0))} = \frac{a_{\bar{\Lambda}}}{z} (1-z)^5 \\
D_{ss}^{\bar{p},\bar{n}} &= \frac{a_{\bar{p}}}{z} (1-z)^{\alpha_R(0)-2\alpha_N(0)+\lambda+2\Delta\alpha+2(1-\alpha_N(0))} = \frac{a_{\bar{p}}}{z} (1-z)^5 \\
D_{ss}^{\bar{\Lambda}} &= \frac{a_{\bar{\Lambda}}}{z} (1-z)^{\alpha_R(0)-2\alpha_N(0)+\lambda+3\Delta\alpha+2(1-\alpha_N(0))} = \frac{a_{\bar{\Lambda}}}{z} (1-z)^{5.5} \\
D_u^{\bar{p},\bar{n}} &= D_d^{\bar{p},\bar{n}} = \frac{a_{\bar{p}}}{z} (1-z)^{-\alpha_R(0)+\lambda+2(1-\alpha_N(0))} = \frac{a_{\bar{p}}}{z} (1-z)^{2.5} \\
D_u^{\bar{\Lambda}} &= \frac{a_{\bar{\Lambda}}}{z} (1-z)^{-\alpha_R(0)+\lambda+\Delta\alpha+2(1-\alpha_N(0))} = \frac{a_{\bar{\Lambda}}}{z} (1-z)^3 \\
D_s^{\bar{p},\bar{n}} &= \frac{a_{\bar{p}}}{z} (1-z)^{-\alpha_R(0)+\lambda+\Delta\alpha+2(1-\alpha_N(0))} = \frac{a_{\bar{p}}}{z} (1-z)^3 \\
D_s^{\bar{\Lambda}} &= \frac{a_{\bar{\Lambda}}}{z} (1-z)^{-\alpha_R(0)+\lambda+2\Delta\alpha+2(1-\alpha_N(0))} = \frac{a_{\bar{\Lambda}}}{z} (1-z)^{3.5}
\end{aligned}$$

References

- [1] J. C. Collins and M. Perry, Phys. Lett. **B34**, 1353 (1975).
- [2] A. M. Polyakov, Phys. Lett. **B72**, 224 (1977).
- [3] S. A. Bass, M. Gyulassy, H. Stöcker, and W. Greiner, INT preprint DOE/ER/40561-11-INT98, hep-ph/9810281 (1998).
- [4] J. Rafelski, Phys. Rep. **88**, 331 (1982).
- [5] B. M. P. Koch and J. Rafelski, Phys. Rep. **142**, 167 (1986).
- [6] M. Gyulassy and W. Greiner, Ann. Phys. **109**, 485 (1977).
- [7] A. Capella, U. Sukhatme, C. I. Tan, and J. T. T. Van, Phys. Rep. **236**, 225 (1994).
- [8] A. Kaidalov, Phys. Lett. **B116**, 459 (1982).
- [9] A. Kaidalov and K. A. Ter-Martirosyan, Phys. Lett. **B117**, 247 (1982).
- [10] A. Capella *et al.*, Z. Phys. C **70**, 507 (1996).
- [11] N. C. T. Alber *et al.*, Z. Phys. C. **64**, 195 (1994).
- [12] N. C. H. Ströbele *et al.*, Nuc. Phys. **A525**, 59c (1991).
- [13] J. D. Bjorken, Phys. Rev. **D27**, 140 (1983).
- [14] E. C. N. N. Biswas, in *Proceedings of the XXI International Symposium on Multiparticle Dynamics* (World Scientific, Singapore, 1992).
- [15] E. C. T. Alexopoulos *et al.*, Phys. Rev. **D46**, 2773 (1992).

- [16] H. J. Möhring, J. Ranft, A. Capella, and J. T. T. Van, Phys. Rev. **D47**, 4146 (1993).
- [17] J. Ranft, A. Capella, and J. T. T. Van, Phys Lett. **B320**, 346 (1994).
- [18] A. Capella, Phys. Lett. **B364**, 175 (1995).
- [19] B. Andersson, G. Gustafson, and B. Nilsson-Almquist, Nucl. Phys. **B281**, 289 (1987).
- [20] C. Hong-Mo *et al.*, Nucl. Phys. **B86**, 470 (1975).
- [21] C. Hong-Mo *et al.*, Nucl. Phys. **B93**, 13 (1975).
- [22] G. F. Chew and C. Rosenzweig, Nucl. Phys. **B104**, 290 (1976).
- [23] G. F. Chew and C. Rosenzweig, Phys. Rep. **41C**, 263 (1978).
- [24] G. F. Chew *et al.*, in *GeV and TeV Hexons from a Topological Viewpoint*, edited by J. T. T. Van (Editions Frontiers, France, 1988).
- [25] G. Veneziano, Nucl. Phys. **B74**, 365 (1974).
- [26] G. 't Hooft, Nucl. Phys. **B72**, 461 (1974).
- [27] E. Witten, Nucl. Phys. **B160**, 57 (1979).
- [28] S. Coleman, in *Pointlike Structure Inside and Outside Hadrons, Erice Lectures*, edited by A. Zichichi (Plenum, New York, 1974), p. 11.
- [29] A. Martin, W. Stirling, and R. Roberts, Phys.Rev. **D50**, 6734 (1994).
- [30] A. Bazarko *et al.*, Z.Phys.C **65**, 189 (1995).
- [31] J. A. Casado, Phys. Lett. **B309**, 431 (1993).
- [32] A. Kaidalov, personal communication.
- [33] A. Capella, A. Kaidalov, C. Merino, and J. T. T. Van, Phys. Lett. **B343**, 403 (1995).
- [34] A. B. Kaidalov, Sov. J. Nucl. Phys. **45**, 902 (1987).
- [35] A. B. Kaidalov and O. I. Piskunova, Z. Phys. C **30**, 154 (1986).
- [36] J. Solano, J. Magnin, and F. R. A. Simao, hep-ex/9710033 (1997), presented at the *5th International Conference on Relativistic Aspects of Nuclear Physic*, 27-29 Aug 1997 , Rio de Janeiro, Brazil.
- [37] A. Capella *et al.*, Z. Phys. C **33**, 541 (1987).
- [38] M. Aguilar-Benitez *et al.*, Z. Phys. C **50**, 405 (1991), the data points shown in this paper were provided to the Durham Reaction Data Database by one of the authors (Y.V.Fisyak).
- [39] H. Kichimi *et al.*, Phys. Lett. **B72**, 411 (1978).

[40] C. W. de Jager, H. de Vries and C. de Vries, *Atomic Data and Nuclear Data Tables* 14, 479 (1974). The author is grateful to N. Armesto for generously providing the code for the computation of the nuclear profile functions.